energy&fuels

pubs.acs.org/EF

Article

Water Saturation and Distribution Variation in Coal Reservoirs: Intrusion and Drainage Experiments Using One- and Two-Dimensional NMR Techniques

Junjian Zhang, Qinhong Hu,* Xiangchun Chang, Zhengyuan Qin,* Xiaoyang Zhang, Stuart Marsh, Stephen Grebby, and Vivek Agarwal

Cite This: *Energy Fuels* 2022, 36, 6130–6143

Read Online

ACCESS | Metrics & More | Article Recommendations

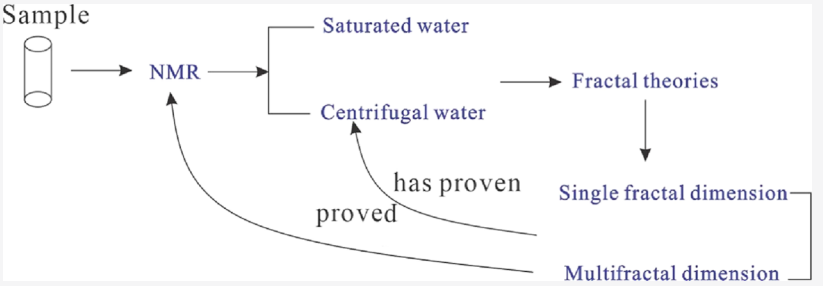

ABSTRACT: Determining water occurrence in pore-fracture systems under specific water saturation is of great significance to reveal the correlation between the water content and porosity/permeability of coal reservoirs. In this work, simulation experiments of water intrusion and drainage are used to study the micro-occurrence and migration of water using NMR T_2 and T_1−T_2 techniques and discuss the influence of pore-fracture system structure parameters on water micro-occurrence. Meanwhile, water distribution heterogeneity in the pore-fracture system is clarified by single- and multifractal theories. The results show that (1) the vacuum saturation method without pressure is unsuitable for high-rank coal samples with micropore development, and water saturation variation leads to a change in significant permeability when water saturation is greater than the critical value, which is related to the coal rank and degree of fracture development; (2) the single-fractal theory can characterize the heterogeneity of water and pore size distribution under static conditions; however, multifractal analyses have a stronger applicability in characterizing water distribution heterogeneity under dynamic conditions; and (3) multifractal parameters have a good correlation with coal sample characteristics such as the water volume in pores and fractures. In the process of centrifugation, both D_{-10}−D_0 and D_{-10}−D_{10} parameters from fractal analyses decrease linearly with a decrease in water content in coal samples, indicating that water distribution heterogeneity in pore-fracture systems decreases with an increase in centrifugal force; and (4) T_2 and two-dimensional spectra in the same coal sample should be comprehensively analyzed as they can quantitatively identify the amount of water migration at different saturation stages.

1. INTRODUCTION

At present, coal-bed methane (CBM) is one of the critical unconventional sources of energy. The accumulation mechanism and dynamic variations in physical properties of the water drainage process in a coal reservoir are the focus of current research.[1−3] During CBM drainage, the water content affects methane adsorption capacity, which controls the reserves of CBM resources.[4−6] During the drainage of CBM, the coal reservoir pressure gradually decreases to the critical desorption pressure with continuous water drainage, causing methane residing in adsorption pores to desorb and migrate through diffusion from the coal matrix to the fractures, which then moves advectively through the fractures to be produced in the wellbore under a pressure differential.[7−9] The essence of CBM production is the process of methane migration and interaction with water under different pressure and temperature conditions in coal reservoirs with pore-fracture networks.[10,11] Therefore, the occurrence and migration characteristics of water are of great significance to interpret CBM accumulation and production.

With increasing activities of CBM exploration and development, current research has gradually changed from the optimization of CBM enrichment and favorable areas toward

Received: March 2, 2022
Revised: May 9, 2022
Published: May 31, 2022

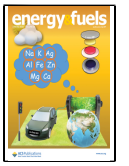

https://doi.org/10.1021/acs.energyfuels.2c00592
Energy Fuels 2022, 36, 6130−6143

CBM production capacity.[12] Therefore, the gas−water interaction in the CBM drainage process is the core content of this work. Many studies in the literature have explained methane adsorption−desorption and permeability variations under different water saturation/content. In general, as the water content (saturation) increases, the adsorption capacity and diffusion rate of methane decrease, and consequently, the gas−water permeability decreases gradually.[13−16] However, there are some uncertainties and limitations in the literature. On the one hand, when water saturation is less than the critical value, the water content has a significant effect on the permeability and diffusion coefficient. On the other hand, this effect is minimum at high water saturation. However, the critical water saturation values of different coal samples are different. Also, water in different coal samples has different effects on gas−water permeability and methane adsorption−desorption, even when the water content is the same among these samples. The reason is that the heterogeneity of the pore-fracture structure leads to differences in the microscopic distribution of water in coal reservoirs. Therefore, determining the content (saturation) of irreducible/movable water [adsorbed/free water (FW)] in coal reservoirs is the basis for a correct understanding of the gas−water interaction.

Low-field nuclear magnetic resonance (NMR) can calculate the water content in the reservoir by detecting hydrogen ions,[17] and this technique has become one of the most common methods for detecting water distribution in various reservoirs. NMR saturation and centrifugal methods are used to calculate the movable and irreducible water saturations of coal reservoirs.[18−22] At a certain centrifugal speed (pressure), water in a coal reservoir can be divided into bound water or immovable water, with the spectral area corresponding to the T_2 spectrum considered as the water content. In addition, the key factors affecting the irreducible water content of coal reservoirs are discussed from the perspective of burial conditions, basic components of coal, the pore-fracture system structure, and other factors.[23−25]

However, the microdistribution of water in coal reservoirs under a certain water saturation still needs to be studied in depth. Moreover, the centrifugal saturation method is only used to divide the occurrence state of water from the aspect of fluidity. Through this method, it is difficult to realize the identification of the multi-state of water such as adsorbed, bound, and movable waters in pore-fracture systems.[20] Under a certain centrifugal pressure, the T_2 spectrum corresponding to the seepage pore or fracture is still developed, indicating that there is still bound water or immovable water in the macropores.[24] Therefore, it is necessary to introduce a new method to identify the microscopic occurrence of water. Related literature indicates that the longitudinal−transverse relaxation (T_1−T_2) technique has been used to obtain more information on the contributions of protons from different water types.[26,27] Based on this technique, five types of water (bound, adsorbed, free, crystal, and structural) in clay minerals were qualitatively identified and described by the specific T_2 to T_1/T_2 ratio values, and T_1−T_2 maps were used to qualitatively indicate the clay types.[25] Song et al.[28] reported that the fluid signals can be divided into FW, bound water in inorganic (BWI) pores, bound water in organic (BWO) pores, and hydrogen-bearing matters in the matrix (HMM) of low-high rank coal samples using T_1/T_2 ratio values.

Above all, the T_1−T_2 technique can identify the micro-occurrence state of water in the reservoir. However, compared with shale, sandstone, and other reservoirs, the application of this technique in fluid identification in coal reservoirs is insufficient. Moreover, there are few studies on the water content of different occurrence states in coal reservoirs under specific water saturation.

In this study, laboratory experiments of water intrusion and drainage were used to study water micro-occurrence and migration using NMR T_2 and T_1−T_2 techniques to determine the water microdistribution under different water saturation. The immovable and movable water saturation values of middle- and high-rank coal samples were calculated by using a saturation and centrifugation method. The factors influencing water micro-occurrence are discussed, such as the pore-fracture system structure and water−air−coal contact angle. Moreover, water distribution heterogeneity in the pore-fracture system is clarified by multifractal theories. The overall results will be helpful in revealing the dynamic migration of water in coal reservoirs in the process of water drainage and CBM production.

2. GEOLOGICAL SETTING OF THE SAMPLING SITE

2.1. Sample Preparation and Experimental Analyses.

The study site is located in the Laochang coal mining area of the eastern Yunnan province in China, which falls in the most important place in southwest China for its CBM enrichment. Eleven fresh coal samples (approximately 15 × 15 × 15 cm^3) were collected from various coal mines, with the results of distribution and basic properties and parameters shown in the study of Zhang et al.[29,30]

Samples were prepared as cylinders and powders of various sizes. Eleven cylindrical cores, each representing a sampling coal mine, with a diameter of 25 mm and a length of 30 or 15 mm were prepared for NMR tests of water intrusion and drainage. Also, 11 powder-sized samples were tested for the pore size distribution by low pressure (LP) CO_2/N_2 gas sorption (GA) by crushing and grinding 7−10 g of coal samples to 40−60 mesh.

For the LP N_2 GA tests, the pore structure was analyzed using the Trostar II model 3020 specific surface area (SSA) and pore size distribution analyzer at a temperature of 77 K. The pore distribution was measured using the Barrett−Joyner−Halenda (BJH) model, and the Brunauer−Emmett−Teller (BET) model was used to describe the SSA of the pores; in addition, detailed information of LP CO_2 GA tests can be found in the study by Zhang et al.[29]

For the water injection and drainage tests using the NMR T_2 and T_1−T_2 spectra, all the samples were placed in a drying oven before the test with the temperature set at 105 °C for approximately 12 h. The dry samples were then weighed (g) using a balance, after which the T_2 spectra and T_1−T_2 spectra of dried samples were measured. After that, the samples were placed under pressure for water saturation and equilibrium for 12 h; the saturated samples were then weighed (g), and T_2 and T_1−T_2 spectra were measured. By adjusting the saturation pressure of coal samples to 5, 10, and 15 MPa sequentially, the mass−T_2−T_1−T_2 spectra of each sample were obtained.

For the water drainage experiments, after the coal sample was saturated under 15 MPa, the pressure associated with the centrifugal speed was adjusted to 0.25, 0.54, 1.50, and 2.87 MPa sequentially. It should be noted that the length of each coal sample was slightly different; therefore, the centrifugal speed of each coal sample was different to achieve the same centrifugal pressure. As mentioned above, for the dry samples, mass−T_2−T_1−T_2 spectra of all the dry samples were measured.

The parameters of the NMR experiment were set as follows during water injection and drainage tests: echo interval time (0.1

https://doi.org/10.1021/acs.energyfuels.2c00592
Energy Fuels 2022, 36, 6130−6143

ms), wait time (4000 ms), number of echoes (12,000), number of scans (64), ambient temperature (25 °C), and number of iterations (10,000). Figure 1 summarizes the experimental methods and testing processes used in this work.

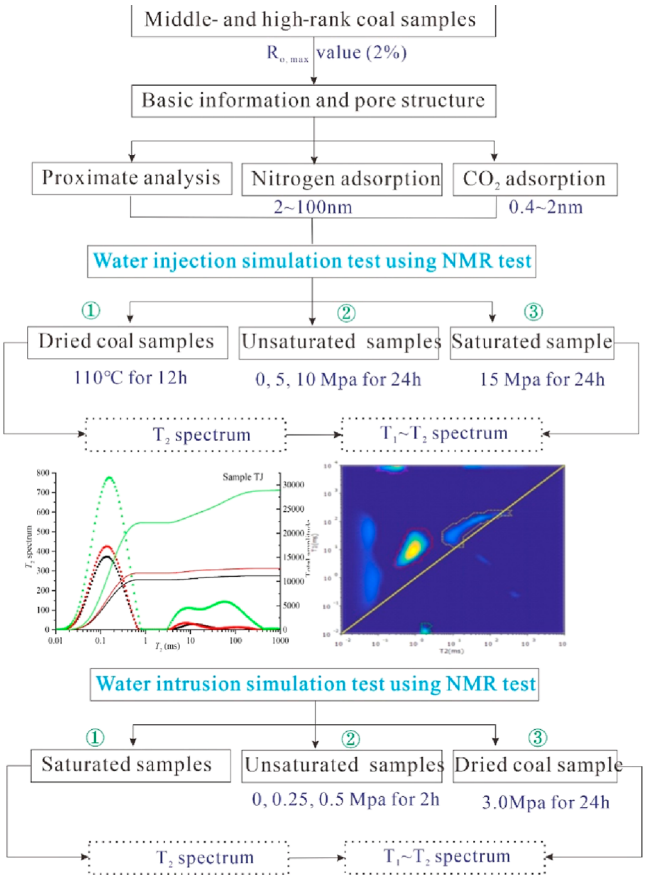

Figure 1. Main experimental methods and testing processes.

2.2. NMR Data Processing and Fractal Theories. NMR can detect the hydrogen content of water and other components (e.g., organic matter and clays) which is divided between dry and wet samples, and consequently, the water content in the pore can be calculated.[31] In this work, Figure 2a is used to analyze the relationship between water quantities and T_2 spectral areas, which shows a good linear and positive correlation. Under a specific water injection pressure/centrifugal speed, the spectral area could be calculated from the T_2 distribution of coal samples, and the water volume in the coal samples was then obtained using the functional relationship $y = 60{,}548.7x + 834.6$.

All the coal samples were heated at high temperatures (110 °C), and then, the T_2 spectrum was measured. Figure 3a shows that the T_2 spectrum of dry samples presents a bimodal distribution, with a smaller T_2 spectral value being developed. It is noted that the spectral area of 2−10 ms is greater than 0, and it is speculated that there may be FW on the wall of the sample tube. In order to compare the T_2 spectral distribution of different coal ranks in the dry state, the parameter spectral area per unit mass (SAPUM) was introduced for comparison.

$$\mathrm{SAPUM} = \mathrm{TSA}/\mathrm{MASS} \tag{1}$$

where TSA represents the total spectral area (arbitrary unit) and MASS is the sample quality, mg.

Figure 3b shows that the SAPUM generally increases with the increase of the $R_{o,max}$ value. The hydrogen content detected from the dry coal samples is expected to come from organic matter such as kerogen. Meanwhile, vitrinite and inertinite content variations will also affect the hydrogen contents. Figure 3c shows that the T_2 spectrum distribution presents a continuously bimodal state when the saturation water pressure is 15 MPa, indicating that the pores and fractures are well connected. By combining Figure 3a,c, the net T_2 spectrum of all coal samples can be obtained (Figure 3d).

To better characterize the effect of saturation pressure on water occurrence and migration, a dimensionless parameter S_{pfi} is defined as

$$S_{pfi} = S_i/S_0 \tag{2}$$

where S_i and S_0 are the spectral areas of T_2 spectra at water saturation drainage pressures (centrifugal speed) P_i and P_0, respectively. In this work, P_0 represents zero saturation pressure (no water saturation pressure), and when I ranges from 1 to 4, the saturation pressure increases from 1 to 5, 10, and 15 MPa, and the centrifugal pressures increase from 0.24 to 0.54, 1.51, and 2.87 MPa, respectively. Overall, a higher value of S_{pfi} indicates less migration and weaker mobility of water.

To better characterize water injection and drainage, a parameter P_M is introduced as

$$P_M = (M_i - M_0)/M_0 \tag{3}$$

where M_i and M_0 are the mass of saturated and dried samples, respectively.

As the lengths of all coal samples are different, different rotational speeds are needed to unify the centrifugal force. The centrifugal pressure difference between two phase flows at specific rotational speeds is equal to the capillary pressure, which is calculated as follows

$$P_{ci} = 1.097 \times 10^{-9} \Delta p L \times (R_e - L/2) \times n^2 \tag{4}$$

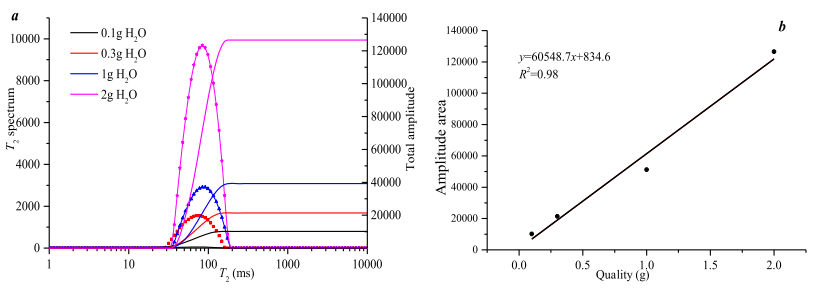

Figure 2. (a) Relationship between water mass and spectral area and (b) water quantity to spectral area conversion.

https://doi.org/10.1021/acs.energyfuels.2c00592
Energy Fuels 2022, 36, 6130−6143

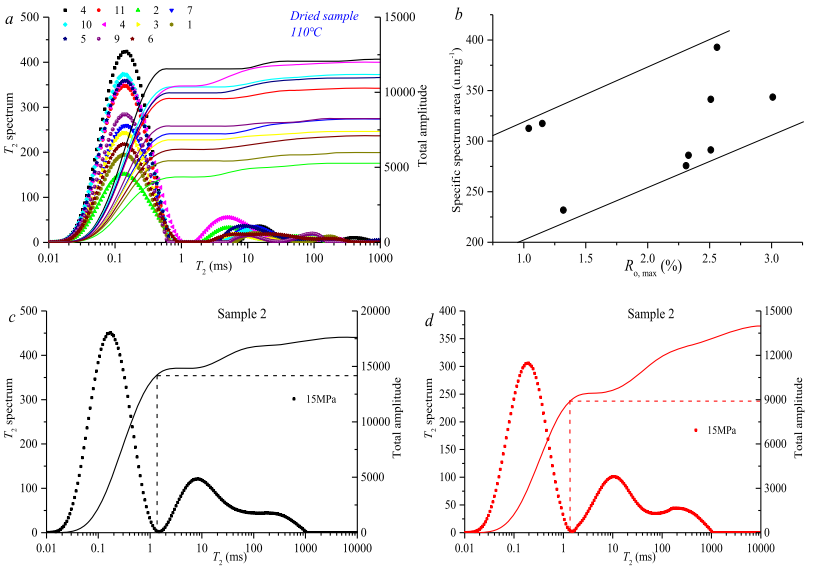

Figure 3. (a) T_2 distribution of dried coal samples; (b) T_2 distribution of coal sample 2; and (c) net T_2 distribution of coal sample 2; (d) the net T_2 spectrum of coal samples.

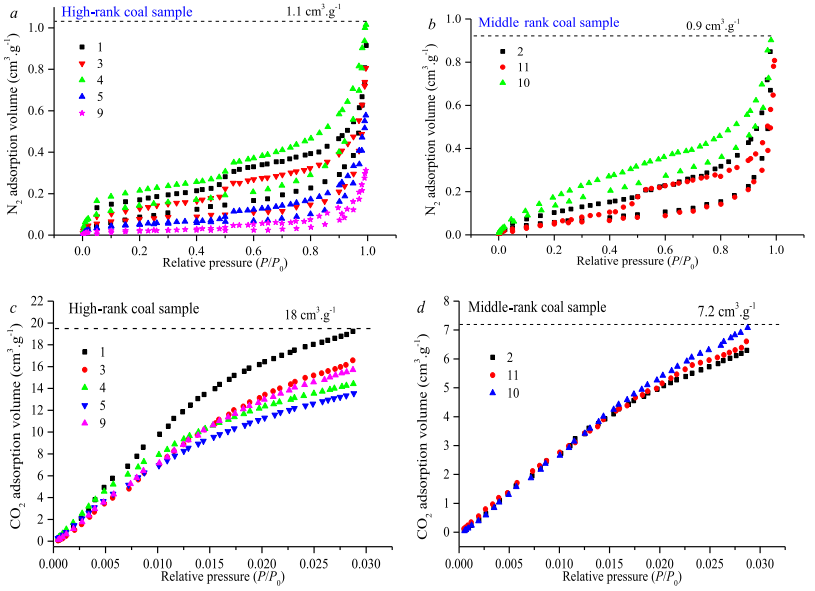

Figure 4. CO_2/N_2 adsorption curves of all 11 coal samples.

where P_{ci} is the centrifugal force, MPa; L is the sample length, cm; R_e is the external rotation radius of the coal sample, cm; Δp is the centrifugal pressure difference between two phase flows, g mL^{-1}; and n is the rotational speed, r min^{-1}.

After the centrifugal force is determined, the corresponding pore diameter is calculated using eq 4.

$$P_{ci} = 2\sigma \cos\theta / r \tag{5}$$

where σ is the air−water interfacial tension, 72 mN/m and θ is the wetting angle, assumed to be 0 °C.

For a quantitative description of water microdistribution, at present, the fractal theory is mainly used to characterize the heterogeneity of pore structure distribution. There are several studies on the characterization of the microscopic distribution heterogeneity of water. In this work, both single- and multifractal models were used to characterize water microdistribution heterogeneity.

According to the specific derivation method found in Zhang et al. (2020b−c), a single-fractal model is defined as

$$\lg(V_p) = (3 - D_w)\lg(T_2) + (D_w - 3)\lg T_{2\,max} \tag{6}$$

where V_p is the percentage of the cumulative pore volume (amplitude) under saturated/unsaturated water (%), T_2 and $T_{2\,max}$ are the transverse relaxation time and maximum lateral relaxation time (ms), respectively, and D_w is the dimensionless NMR fractal dimension of specific water distribution.

Multifractal models are defined as the singularity indices a and $f(a)$ obtained using eqs 6 and 8, which can be expressed as

$$a(q) \propto \frac{\sum_{i=1}^{N(\varepsilon)} [u_i(q, \varepsilon)\lg \varepsilon]}{\lg \varepsilon} \tag{7}$$

https://doi.org/10.1021/acs.energyfuels.2c00592
Energy Fuels 2022, 36, 6130−6143

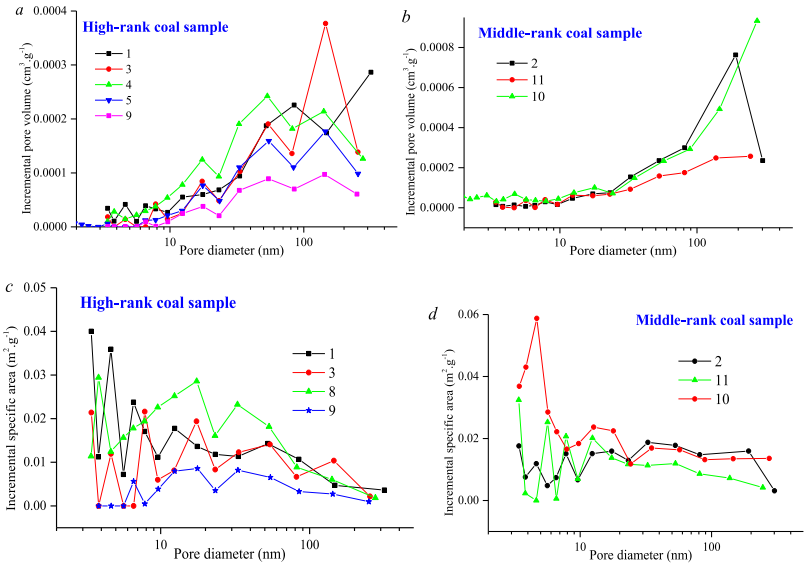

Figure 5. Pore size distributions obtained from N_2 adsorption tests.

Table 1. Water Content (g) Variation during Injection

sample no.	$Ro_{,max}$ (%)	mass of dried samples (g)	equilibrium water condition	saturation pressure (0.10 MPa)	saturation pressure (5 MPa)	saturation pressure (10 MPa)	saturation pressure (15 MPa)
1	3.01	17.41	17.73	18.52		18.60	18.61
2	1.32	22.73	22.81	22.97		23.02	23.04
3	2.56	18.81	19.02	19.31		19.43	19.45
4	2.51	41.18	41.47	42.64		42.68	42.69
5		32.76	32.92	33.71	33.74	33.75	33.76
6	2.33	38.15	38.38	39.24	39.24	39.24	39.26
7	2.33	38.87	39.08	39.90		39.92	39.93
8	2.51	35.73	36.02	37.12	37.13	37.14	37.14
9	2.31	34.97	35.20	36.42		36.55	36.58
10	1.15	35.21	35.28	35.56	35.61	35.62	35.63
11	1.34	32.86	33.05	33.47		33.65	33.67

$$f(a) \propto \frac{\sum_{i=1}^{N(\varepsilon)} [u_i(q, \varepsilon) \lg u_i(q, \varepsilon)]}{\lg \varepsilon} \tag{8}$$

$$u_i(q, \varepsilon) = \frac{p_i^q(\varepsilon)}{\sum_{i=1}^{N(\varepsilon)} p_i^q(\varepsilon)} \tag{9}$$

where the curve consisting of a and $f(a)$ is called the multifractal singularity spectrum and q is the order of the statistical matrix. When $q \gg 1$, the information of higher probability areas is amplified; when $q \ll 1$, the information of lower probability areas is amplified. In this study, q lies between $[-10,10]$ with a step of 1. a and $f(a)$ can be acquired by linear regression of the two equations.

The characteristic parameters of $f(a)$ mainly include a_{min}, a_{max}, a_0, a_0-a_{max}, $a_{min}-a_0$, and A, and the detailed description can be found in the literature given above. The other set $q \sim D(q)$ is introduced from the perspective of an information theory called generalized fractal dimension, and a detailed description can be found in Zhang et al.[22,25]

3. RESULTS AND DISCUSSION

3.1. Pore-Fracture System of All Coal Samples. Figure 4 shows that the N_2 adsorption volume of the middle-rank coal sample is smaller than that of the high-rank coal sample. Then, adsorption and desorption curves of middle-rank coal with pore sizes larger than 10 nm nearly overlap, where semiclosed pores are generally developed (Figure 4a). In contrast to that of the middle-rank coal, the adsorption−desorption curve of high-rank coal samples has a significant adsorption loop at p/p_0 values higher than 0.8, indicating that samples with pores larger than 10 nm are dominated by open pores (parallel platelets) and that the pore morphology is similar (Figure 4b). Moreover, the CO_2 adsorption volume of a high-rank coal sample is between 12 and 19 $cm^3\ g^{-1}$, which is larger than that of a middle-rank coal sample (6−7.2 $cm^3\ g^{-1}$).

The pore-fracture system of all coal samples with pore diameters of 2−100 nm shows that the pore volume of 50−100 nm in high-rank coal samples is more than 50%, which provides a large proportion of pore volume and also SSA at pore sizes of 2−100 nm (Figure 5a,b). However, the pore volume of 2−10 nm in middle-rank coal samples is more than 60%, which provides a large proportion of pore volume and SSA of 2−100 nm (Figure 5c,d). The pore-fracture system with pore sizes less than 2 nm of all the samples shows a multipeak distribution of pore volume and SSA. The distribution of pore volume and SSA of micropores in high-rank coal samples is bimodal with the peak position at 0.5 and 0.65 nm. However, the pore volume and SSA distributions of the micropores in middle-rank coal samples exhibit three peaks with the peak points at 0.5, 0.65, and 0.80

https://doi.org/10.1021/acs.energyfuels.2c00592
Energy Fuels 2022, 36, 6130−6143

Table 2. Water Content (g) Variation during Drainage

sample no.	mass of dried samples (g)	saturation pressure (15 MPa)	centrifugal pressure (0.24 MPa)	centrifugal pressure (0.54 MPa)	centrifugal pressure (1.51 MPa)	centrifugal pressure (2.87 MPa)
10	35.21	35.6242	35.5152	35.4799	35.474	35.4561
9	34.97	36.5774	36.1371	35.9345	35.8537	35.7136
11	32.86	33.6455	33.3899	33.3021	33.2436	33.1615
5	32.76	33.7615	33.6424	33.5785	33.5402	33.4667
3	18.81	19.450	19.3778	19.3317	19.2952	19.2704
2	22.73	23.039	22.9711	22.9452	22.9274	22.9191
1	17.41	18.5998	18.4254	18.0937	17.9837	17.9111
J1		16.3993	16.371	16.352	16.3427	16.3322

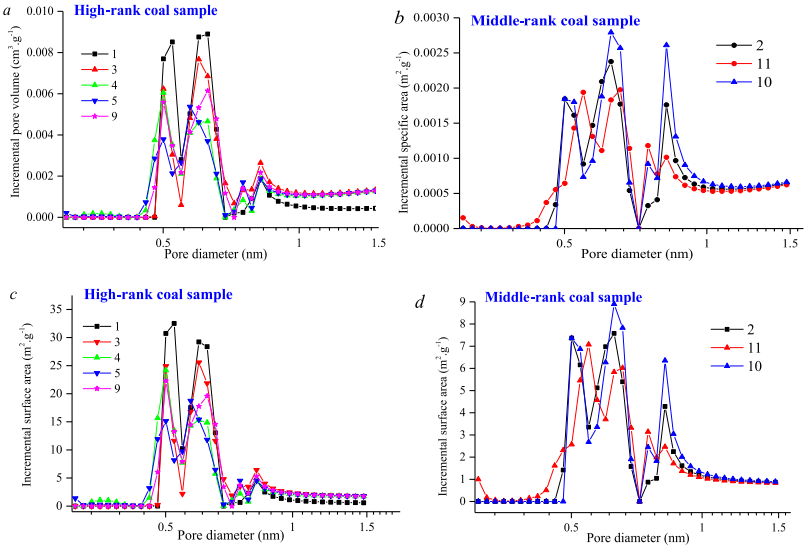

Figure 6. Pore size distributions obtained from CO_2 adsorption tests.

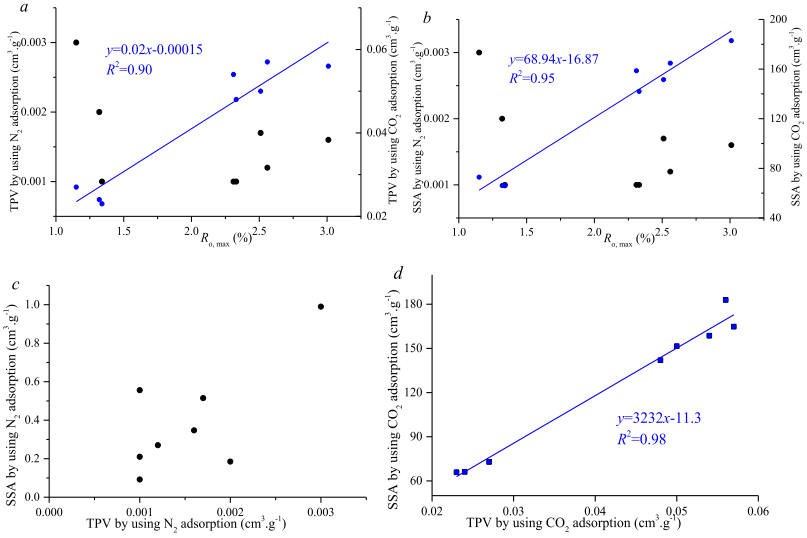

Figure 7. Relationship between the TPV and SSA found by using CO_2/N_2 adsorption tests.

nm, respectively. This is also why the pore volume and SSA of high-rank coal are much larger than those of middle-rank coal.

By using the CO_2/N_2 adsorption curve, the total pore volume (TPV) and SSA of all coal samples can be obtained. The TPV and SSA found by using N_2 adsorption curves are smaller than that by using CO_2 adsorption curves. Pores with a size less than 2 nm provide a large proportion of the volume and SSA of nanopores. Compared with the pore structure of 2−100 nm, the volume and SSA of pores <2 nm increase linearly as $R_{o,max}$ increases (Figure 5a,b). Meanwhile, there is a good linear relationship between the SSA and TPV of micropores with a size less than 2 nm, but the correlation between the SSA and TPV of the mesopores with a size of 2−100 nm is weak (Figure 5c,d).

3.2. Water Micro-Occurrence and Migration during Water Intrusion. With the increase of saturation pressure, the mass of each coal sample increases gradually (Table 1). When

https://doi.org/10.1021/acs.energyfuels.2c00592
Energy Fuels 2022, 36, 6130−6143

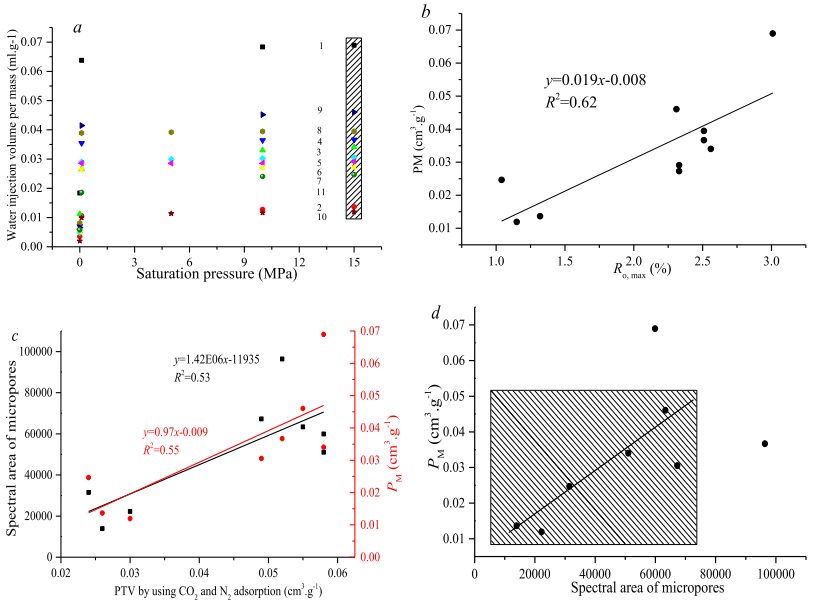

Figure 8. Relationship between saturation pressure and water volume of pore-fracture systems.

the saturation pressure is less than 0.1 MPa, the water injective volume is larger (Figures 6 and 7). When the saturation pressure is greater than 0.1 MPa, the water injective volume remains stable (Figure 8a), indicating that coal reservoirs have strong wettability, and the coal sample can basically reach saturation under low water injection pressure. The injected volume per unit mass, P_m, and $R_{o,max}$ have an obviously linear positive correlation, that is, the injective capacity of the high-rank coal sample is greater than that of the middle-rank coal sample (Figure 8b). On the one hand, micropores of coal samples are developed with increasing coal rank, and then, the TPV of each sample increases, resulting in an increase in water adsorption capability (Figure 8c,d). On the other hand, the high-rank coal sample has a stronger wettability, which leads to the enhancement in water adsorption ability. It is noted that there is no obvious linear positive correlation between P_M and the micropore spectral area. The reason is that P_M includes water in micropores, seepage pores, and fractures. For the coal with developed fractures, water in the fractures also controls the P_M value variation.

In this equilibrium water condition, the T_2 spectrum of the coal sample shows a single peak distribution, and water mainly exists in micropores. Under this condition, water is mainly evaporated and dissipated, and water in the fracture is evaporated in the process (Figure 9). In the process of vacuum saturation, water is evenly distributed in the pore-fracture system with the increase of saturation pressure. When the saturation pressure is greater than 0.1 MPa, the water content in the micropores varies obviously, and water fully saturates the fractures. This also shows that the method of vacuum saturation for coal samples in relevant literature still needs to be discussed. The vacuum saturation method is unsuitable for high-ranking coal samples with well-developed micropores even though it can be applicable for conventional sandstone reservoirs.

The T_2 spectra of all coal samples at a water pressure of 15 MPa are shown in Figure 9. Zhang et al.[15] and Zou et al.[18] classified the pore-fracture system into adsorption pores ($0-10^2$ nm, $T_2 < 2.5$ ms), seepage pores (10^2-10^4 nm, 2.5 ms $< T_2 <$ 50 ms), and fractures ($>10^4$ nm, $T_2 >$ 100 ms) using the T_2 spectrum and the response characteristics (relaxation time) of different pore diameters. This work refers to the division scheme given in the study of Yao et al.,[17] with the classification of adsorption pores, seepage pores, and fractures based on the T_2 spectrum. According to the T_2 distribution, all samples can be divided into these three types. As shown in Figure 9, samples FZ and TC15 belong to Type I as their T_2 spectra show a continuous three-peak model, which shows that its pore-fracture system is relatively well developed, and the connectivity is better than that in other types. Many samples belong to Type II, and the three-peak mode is also developed for their T_2 spectra. In this case, the area of the main peak is larger than that of the other two subpeaks that are separated from each other, indicating that the adsorption and seepage pores are poorly connected. Furthermore, sample 3 belongs to Type III; its T_2 spectrum shows a two-peak mode, and its fracture is undeveloped. Moreover, there exists an interval between adsorption and seepage peaks that also indicates a poor connectivity between these two groups of pores.

Figure 10a shows that the water volume of the pore-fracture system in high-rank coal samples (0.03−0.08 cm^3 g^{-1}) is much greater than that of middle-rank coal samples (0.008−0.02 cm^3 g^{-1}). Among them, the pore volume of micropores gradually increases as the coal rank increases. However, the water content of the seepage pores gradually decreases as the degree of coal metamorphism increases (Figure 10b). It is noted that a large number of microfractures are generated in coal samples when $R_{o,max}$ is about 2%, resulting in the development of microcracks in middle-rank coal samples, that is, a spectral area of a T_2 spectrum greater than 100 is relatively developed (samples 2, 11, J1, and 10).

3.3. Water Migration during Water Drainage. *3.3.1. Water Volume Variation.* Water volumes of all the saturated coal samples are shown by the functional relationship given in Figure 3. As the centrifugal pressure increases, the water content of the pore-fracture system decreases. Under the same centrifugal pressure, the spectral area declining rate of water in the fracture is relatively large. When the centrifugal force exceeds 1.50 MPa, the decreasing rate of the water content in micropores increases, while the water content in seepage pores and fractures remains unchanged. It should be noted that the spectral area of micropores in sample 2 increases when the centrifugal force is

https://doi.org/10.1021/acs.energyfuels.2c00592
Energy Fuels 2022, 36, 6130−6143

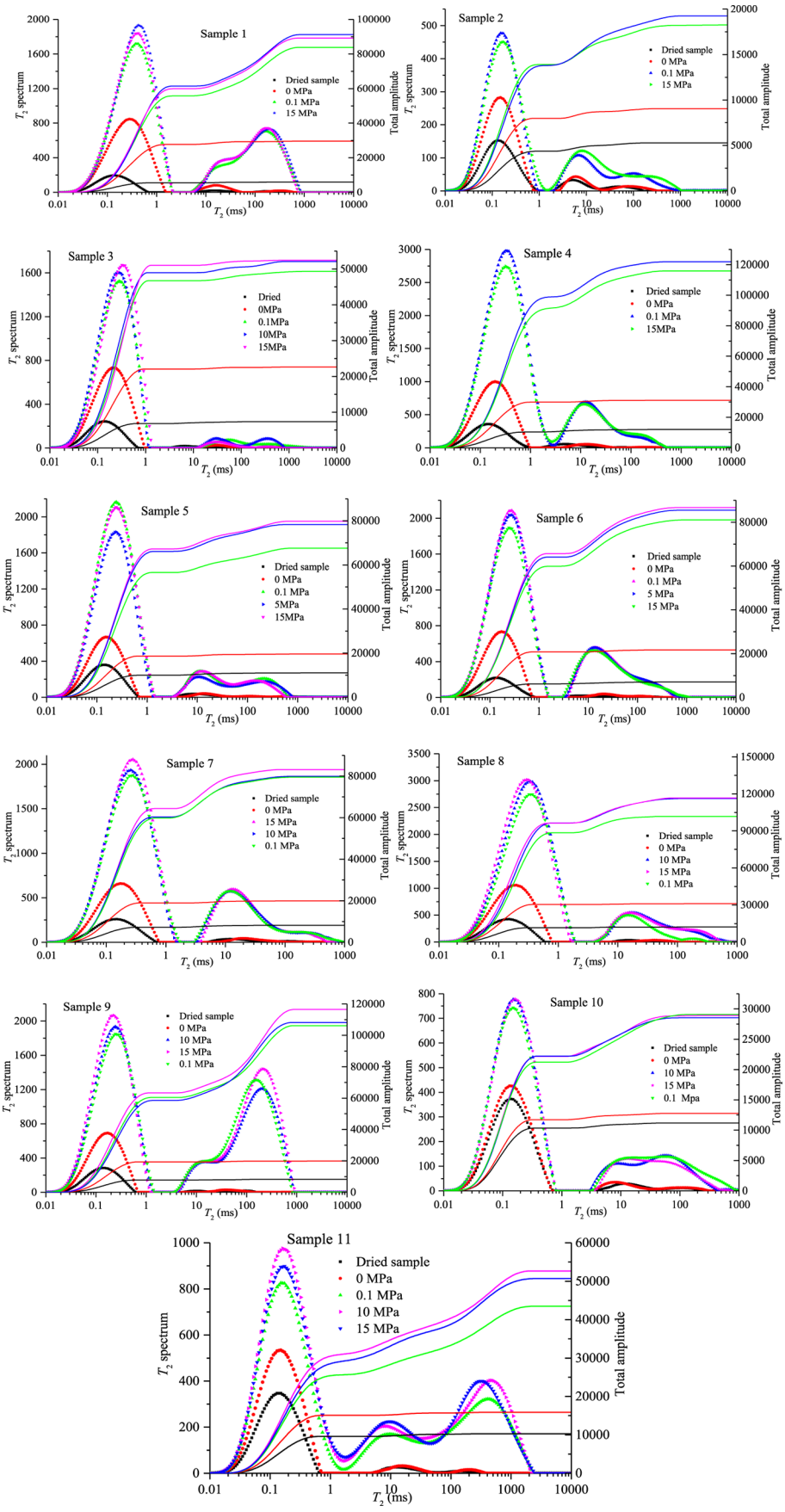

Figure 9. T_2 spectrum distributions of all the samples at different saturation pressures.

https://doi.org/10.1021/acs.energyfuels.2c00592
Energy Fuels 2022, 36, 6130−6143

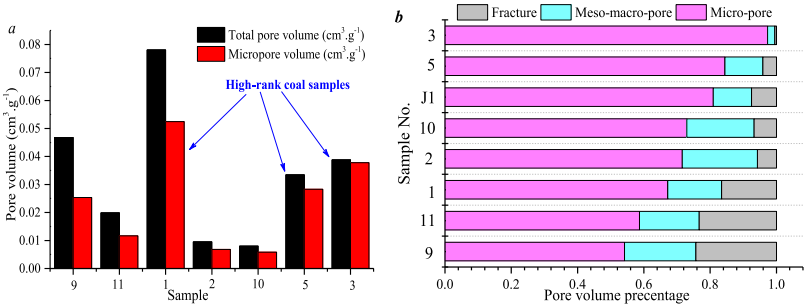

Figure 10. Pore volume percentages calculated by using saturated T_2 spectrum distributions.

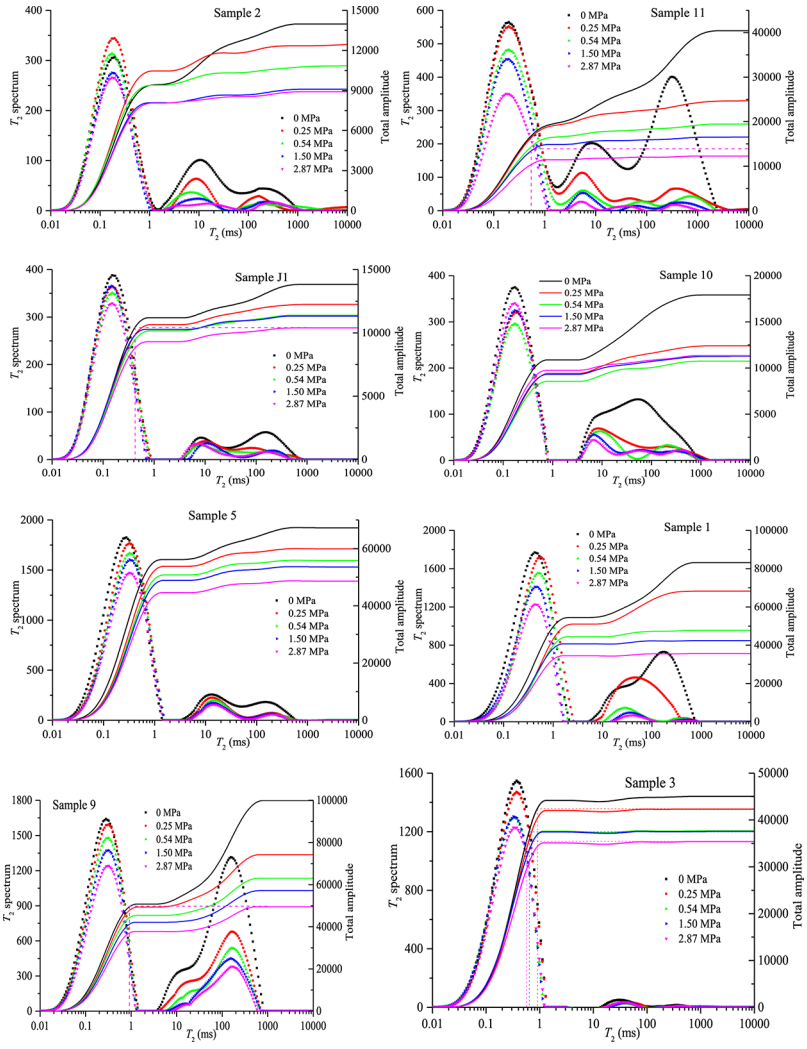

Figure 11. T_2 spectrum distributions of all the samples under different centrifugal pressures.

0.25 MPa, while the spectral area of fractures decreases. This phenomenon mainly occurs in low- and middle-rank coal samples; this could be related to the fact that the micropores of this type of coal sample are not developed, and the transformation effect of micropores and mesopores is relatively obvious.[32]

When the maximum centrifugal pressure is 2.87 MPa, the corresponding centrifugal pore size is 60 nm (eqs 3 and 4). After the centrifugal test was completed, S_{pi} of all the samples was found to be between 0.4 and 0.82. This shows that the water saturation of each coal sample after centrifugation is 40−82% (Figure 12a). As the centrifugal pressure increases, the water content in the micropores, seepage pores, and fractures decreases exponentially. Combining Figure 12b−d, S_{pi} of micropores, seepage pores, and fractures of all the samples is 0.65−0.95, 0.10−0.65, and 0−0.46, respectively. This is mainly because the maximum centrifugal force cannot overcome part of the capillary force of micropores, resulting in a smaller water content variation in the micropores.

3.3.2. Influence of the Mechanism of Water Saturation on Transmission in the Pore-Fracture System. For sample 11 with a fracture development, when the water saturation decreases from 100 to 57% (the centrifugal pressure is less than 0.54 MPa), it is mainly related to the change in water content in fractures.

https://doi.org/10.1021/acs.energyfuels.2c00592
Energy Fuels 2022, 36, 6130−6143

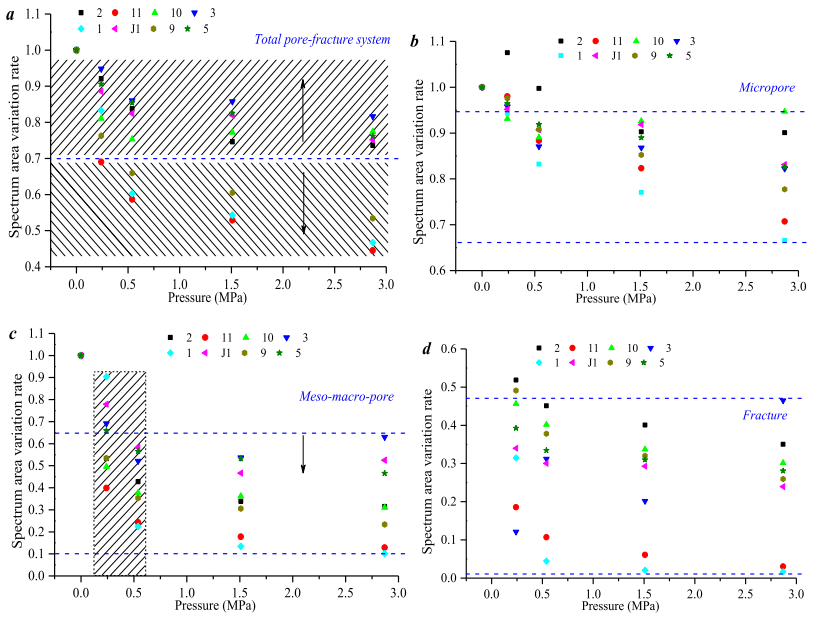

Figure 12. Water content variations in adsorption and seepage pores and fractures during water drainage.

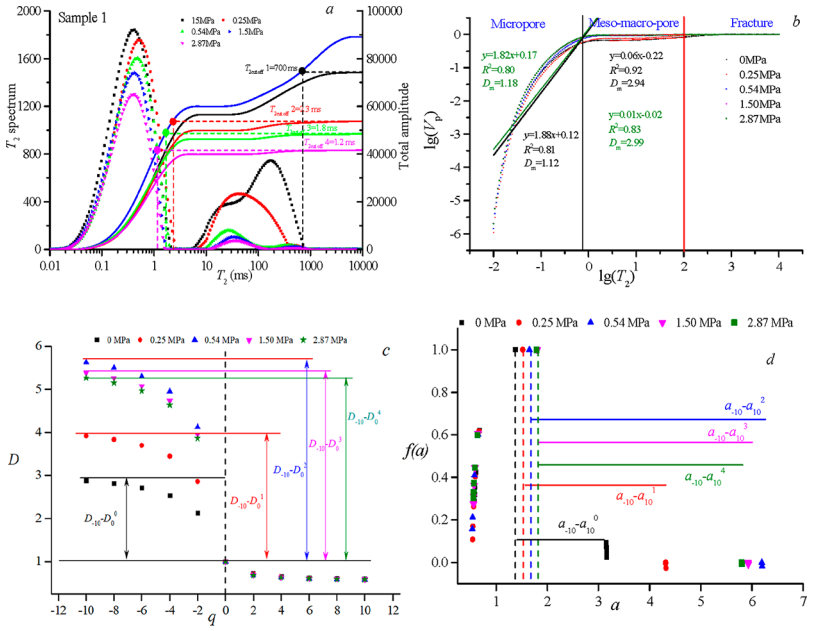

Figure 13. (a) T_2 spectrum distribution at different centrifugal pressures; (b) water microdistribution heterogeneity calculated by using single fractal models; and (c,d) water microdistribution heterogeneity calculated by using multifractal models.

The development of fractures in the coal sample significantly affects the permeability variation. At this initial stage, water saturation variation results in remarkable permeability changes. When the water saturation decreases from 57 to 42% (the centrifugal pressure is larger than 0.54 MPa), it is related to water content variation in micropores (Figure 11). The water content of micropores has a weak effect on permeability. At this late stage, the influence of water saturation on permeability variation is weak. It indicates that the water saturation has a stage effect on the permeability variation. There is critical water saturation $S_{critical}$ in the coal sample with developed fractures. When the water saturation value is greater than this value, water saturation variation leads to a significant variation in permeability. When the water saturation is less than this value, the change in water saturation is not obvious in the permeability variation. In Figure 11, $S_{critical}$ of samples 11, J1, and 1 is 57, 83, and 59%, respectively. This value is mainly related to the volume percentage of the fracture. In general, the volume percentage of the fracture is inversely proportional to this value.

For coal sample 3 with micropores developed, with the increase of centrifugal pressure, the variation in water saturation is related to the water content of micropores. The initial permeability of this type of sample is smaller, and the effect of water saturation on the permeability variation is weak. Therefore, there is no critical water saturation for this type of sample.

The overall results from this work explain the dynamic variation in porosity and permeability under different water

https://doi.org/10.1021/acs.energyfuels.2c00592
Energy Fuels 2022, 36, 6130−6143

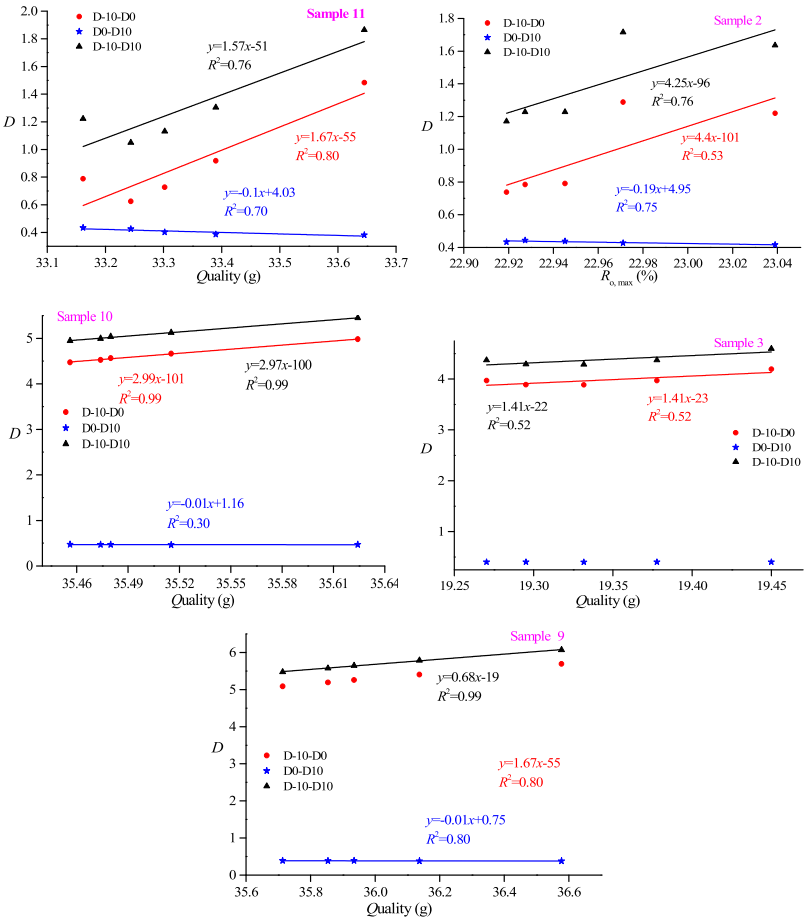

Figure 14. Correlation between multifractal parameters and quality variation of typical samples.

saturation conditions. In different coal samples, microscopic water occurrence under the same water saturation is obviously different.

3.3.3. Water Distribution Heterogeneity Variation in Pore-Fracture Systems. Equations 5−8 are used to calculate the water distribution heterogeneity in the pore-fracture system under different centrifugal pressures, taking sample 1 as an example (Figure 13a). Single-fractal calculation results show that the fractal dimension variation is weak under different centrifugal pressures, and water distribution heterogeneity in micropores is relatively strong (Figure 13b). The fractal dimension variation of water distribution in adsorption pores, seepage pores, and fractures is about 0.01, indicating that the heterogeneity of water distribution remains stable under the effect of centrifugal force. It has been proven that a single-fractal dimension is a better method to characterize the nanopore size distribution. However, it is worth noting that the applicability of single-fractal analyses to quantitatively characterize pore size distribution heterogeneity under different temperature and pressure conditions remains to be discussed. Related literature shows that single fractals were used to study the fractal dimension variation among the same samples under different experimental conditions (temperature, pressure, and time).[28,29,32−35] The results indicate relatively minor differences between fractal dimension values, which also affects the accuracy of these results. In conclusion, the single-fractal analyses will not sufficiently reflect the dynamic variation of water distribution heterogeneity as shown in this work.

Figure 13c,d shows that the multifractal dimension of water distribution in a pore-fracture system varies significantly under different centrifugal pressures. The results show that q versus $D(q)$ spectra of all samples have a distinct reversely shaped curve, and the a versus $f(a)$ spectra of all samples clearly have a parabolic-shaped distribution. Then, the D_0-D_{10} value is smaller than $D_{-10}-D_0$ in one sample, and a_0-a_{10} is smaller than $a_{-10}-a_0$, indicating that lower probability measure areas control the overall water distribution heterogeneity of the pore-fracture system (Figure 13c,d). With the increase of centrifugal pressure, $D_{-10}-D_0$ and $a_{-10}-a_0$ decrease, indicating that water distribution heterogeneity of lower probability measure areas gradually decreases. The principle of the multifractal equation mainly determines this phenomenon. Combining Figures 5 and 13, lower probability measure areas mainly correspond to seepage pores and fractures. Under the effect of centrifugal pressure, the variation in water content in the fracture is the largest, so $D_{-10}-D_0$ of lower probability measure areas varies greatly. Compared with Figure 13b, the multifractal model has a stronger applicability in characterizing the microdistribution heterogeneity of water.

Figure 14 shows that multifractal parameters have a good correlation with coal sample quality (water volume in pores and fractures). In the process of centrifugation, $D_{-10}-D_0$ and $D_{-10}-D_{10}$ decrease linearly with the decrease of water content in coal samples. However, D_0-D_{10} increase as the centrifugal force increases linearly. This indicates that water distribution heterogeneity in the pore-fracture system decreases with the increase of centrifugal force. Meanwhile, there is a linear

https://doi.org/10.1021/acs.energyfuels.2c00592
Energy Fuels 2022, 36, 6130−6143

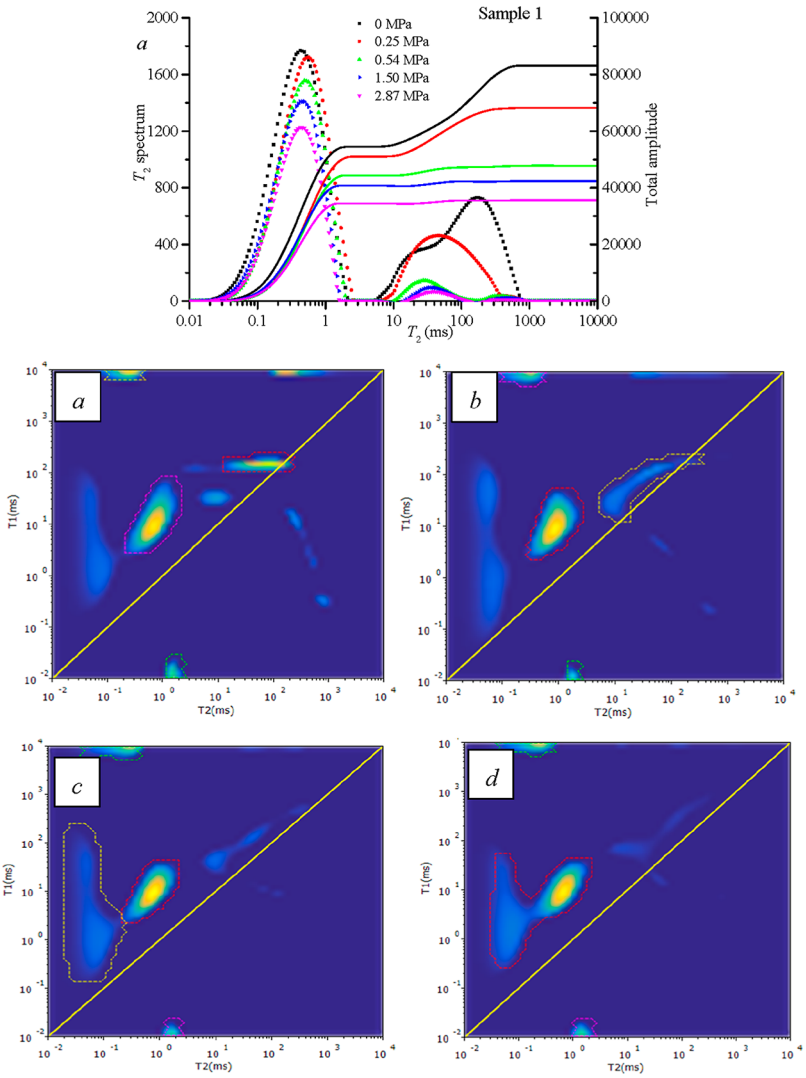

Figure 15. T_1−T_2 spectrum variations of sample 1 at different centrifugal pressures. (a) 0, (b) 0.25, (c) 0.54, and (d) 1.50 MPa.

relationship between the sample quality and multifractal parameters.

$$D = ax + b$$

where D is the value of D_{-10}−D_0 and D_{-10}−D_{10}; x is the quality, g; and a and b are constants.

It is well known that there is a linear relationship between mass and water saturation (S_{water}).

$$D = aS_{water} + b$$

Figure 14 shows that the value of a is between 0.68 and 4.25, which is related to the pore volume and pore connectivity.

3.4. Water Micro-Occurrence during Water Migration Using the T_1−T_2 Spectrum. The water occurrence states under different centrifugal states are analyzed using T_1−T_2 spectra. According to the results presented in this paper and the results in the study of Yao et al.,[17] the fluid signals can be divided into FW, BWI pores, BWO pores, and HMM. When the centrifugal force is 0.25 MPa, the spectrum with a T_2 of 10−1000 ms of sample 1 gradually decreases, indicating that the water content of the seepage pores and fractures decreases (Figure 11). Meanwhile, the area ratio of two-dimensional spectra (T_2 = 10−100 ms, T_1 = 10−100 ms) decreases, which indicates that this range corresponds to FW in seepage pores and fractures. According to eqs 4 and 5, the centrifugal pore diameter under the effect of the centrifugal force is 1200 nm, which is consistent with the previous conclusions. When the centrifugal force reaches 0.54 and 1.54 MPa, respectively, the corresponding centrifugal diameter limit is 200 nm. In this state, the FW content decreases, and the spectral area corresponding to 10−100 ms in the T_2 spectrum is smaller. Meanwhile, it is noted that the T_2 spectrum in the seepage pore does not completely disappear, which is caused by the complex pore structure of some seepage pores.

When the centrifugal force is greater than 0.54 MPa, the water in the adsorption pore (T_2 < 2.5 ms) is mainly discharged (Figure 15a). It indicates that this stage is dominated by the discharge process of bound water.[28] This also proves that the adsorption pore mainly contains adsorbed water. Meanwhile, two separate regions (regions 1 and 2) in the two-dimensional spectra gradually merge into a continuous whole. Comparing Figure 15d,e, it can be seen that the drainage process of bound water can be divided into two stages, that is, inorganic pore-bound water and organic pore-bound water. Figure 15e shows that water in the coal sample is mainly BWO matter after the centrifugation process, which is distributed in the adsorption pores. At the same time, the spectral signal in this state also

https://doi.org/10.1021/acs.energyfuels.2c00592
Energy Fuels 2022, 36, 6130−6143

includes the hydrogen signal in kerogen, but the signal quantity in this region is relatively low.

CONCLUSIONS

In this work, laboratory experiments of water intrusion and drainage were used to study water micro-occurrence and migration using NMR T_2 and T_1-T_2 techniques in addition to gas sorption results for pore structure characterization. The factors influencing water micro-occurrence are discussed, such as the pore structure parameters and coal wettability. Meanwhile, water distribution heterogeneity in the pore-fracture system is clarified by applying multifractal theories to interpret the data. The main conclusions are presented as follows:

(1) When the saturation pressure is greater than 0.1 MPa, the water content in the micropores varies obviously, and water fully saturates the fractures. The vacuum saturation method without pressure is unsuitable for high-ranking coal samples with micropore development.

(2) There is a critical water saturation value $S_{critical}$. When water saturation is greater than this value, water saturation variation leads to a significant percolation variation. When water saturation is less than this value, water saturation variation is not evident for the percolation variation. For different coal samples, microscopic water occurrence under the same water saturation is different.

(3) The single-fractal model does not sufficiently reflect the dynamic variation of water distribution heterogeneity, while the multifractal model has a stronger applicability. This indicates that water distribution heterogeneity in the pore-fracture system decreases with an increase in centrifugal force. Meanwhile, there is a linear relationship between the sample quality and multifractal parameters.

(4) In centrifugation, FW is discharged first, followed by BWI matter, and finally, BWO matter. It is suggested that the T_2 and two-dimensional spectra in the same sample should be comprehensively analyzed in order to quantitatively identify the water migration amount at different stages.

AUTHOR INFORMATION

Corresponding Authors

Qinhong Hu − *Department of Earth and Environment Sciences, University of Texas at Arlington, Arlington, Texas 76019, United States;* orcid.org/0000-0002-4782-319X; Email: maxhu@uta.edu

Zhengyuan Qin − *Nottingham Geospatial Institute, Faculty of Engineering, University of Nottingham, Nottingham NG7 2TU, U.K.;* orcid.org/0000-0002-4967-0377; Email: zhengyuan.qin@nottingham.ac.uk

Authors

Junjian Zhang − *College of Earth Sciences & Engineering, Shandong University of Science and Technology, Qingdao 266590, China; Key Laboratory of Coalbed Methane Resource & Reservoir Formation Process, Ministry of Education, China University of Mining and Technology, Xuzhou 221008, China; School of Resources and Earth Science, China University of Mining and Technology, Xuzhou 221116, China;* orcid.org/0000-0001-7557-4306

Xiangchun Chang − *College of Earth Sciences & Engineering, Shandong University of Science and Technology, Qingdao 266590, China*

Xiaoyang Zhang − *College of Earth Sciences & Engineering, Shandong University of Science and Technology, Qingdao 266590, China;* orcid.org/0000-0002-1735-1443

Stuart Marsh − *Nottingham Geospatial Institute, Faculty of Engineering, University of Nottingham, Nottingham NG7 2TU, U.K.*

Stephen Grebby − *Nottingham Geospatial Institute, Faculty of Engineering, University of Nottingham, Nottingham NG7 2TU, U.K.*

Vivek Agarwal − *Nottingham Geospatial Institute, Faculty of Engineering, University of Nottingham, Nottingham NG7 2TU, U.K.*

Complete contact information is available at: https://pubs.acs.org/10.1021/acs.energyfuels.2c00592

Notes

The authors declare no competing financial interest.

ACKNOWLEDGMENTS

This research was sponsored by the Natural Science Foundation of Shandong Province, China (nos. ZR2021QD072 and ZR2020QD040), and the Major National Science and Technology Projects (no. 2016ZX05044002-003).

REFERENCES

(1) Yu, S.; Bo, J.; Ming, L. A review on pore-fractures in tectonically deformed coals. *Fuel* **2020**, *278*, 118248.

(2) Wang, G.; Qin, X.; Han, D.; Liu, Z. Study on seepage and deformation characteristics of coal microstructure by 3D reconstruction of CT images at high temperatures. *Int. J. Min. Sci. Technol.* **2021**, *31*, 175−185.

(3) Tao, S.; Chen, S.; Pan, Z. Current status, challenges, and policy suggestions for coalbed methane industry development in China: A review. *Energy Sci. Eng.* **2019**, *7*, 1059−1074.

(4) Wu, J.; Yu, J.; Wang, Z.; Fu, X.; Su, W. Experimental investigation on spontaneous imbibition of water in coal: Implications for methane desorption and diffusion. *Fuel* **2018**, *231*, 427−437.

(5) Song, Y.; Jiang, B.; Wei, C. A review on the application of molecular dynamics to the study in coalbed methane geology. *Front. Earth Sci.* **2021**, *9*, 775497.

(6) Shen, J.; Zhao, J.; Qin, Y.; Shen, Y.; Wang, G. Water imbibition and drainage of high rank coals in Qinshui Basin, China. *Fuel* **2018**, *211*, 48−59.

(7) Li, H.; Lin, B.; Chen, Z.; Hong, Y.; Zheng, C. Evolution of coal petrophysical properties under microwave irradiation stimulation for different water saturation conditions. *Energy Fuels* **2017**, *31*, 8852−8864.

(8) Liu, X.; Wu, C. Simulation of dynamic changes of methane state based on NMR during coalbed methane output. *Fuel* **2017**, *194*, 188−194.

(9) Tan, Y.; Pan, Z.; Liu, J.; Kang, J.; Zhou, F.; Connell, L. D.; Yang, Y. Experimental study of impact of anisotropy and heterogeneity on gas flow in coal. Part I: Diffusion and adsorption. *Fuel* **2018**, *232*, 444−453.

(10) Liu, S.; Harpalani, S.; Pillalamarry, M. Laboratory measurement and modeling of coal permeability with continued methane production: Part 2-Modeling results. *Fuel* **2012**, *94*, 117−124.

(11) Zhang, J.; Wei, C.; Yan, G.; Lu, G. Structural and fractal characterization of adsorption pores of middle-high rank coal reservoirs in western Yunnan and eastern Guizhou: An experimental study of coals from the Panguan syncline and Laochang anticline. *Energy Explor. Exploit.* **2019**, *37*, 251−272.

(12) Qin, Y.; Tim, M.; Shen, J.; Yang, Z.; Shen, Y.; Wang, G. Resources and geology of coalbed methane in China: A review. *Int. Geol. Rev.* **2018**, *60*, 777−812.

(13) Li, J.; Lu, S.; Cai, Y.; Xue, H.; Cai, J. Impact of coal ranks on dynamic gas flow: An experimental investigation. *Fuel* **2017**, *194*, 17−26.
(14) Zong, Y.; Han, L.; Meng, Q. W. Strength properties and evolution laws of cracked sandstone samples in re-loading tests. *Int. J. Min. Sci. Technol.* **2020**, *30*, 251−258.
(15) Zhang, J.; Wei, C.; Ju, W.; Qin, Z.; Ji, Y.; Quan, F.; Hu, Y. Microscopic distribution and dynamic variation of water under stress in middle and high rank coal samples. *J. Nat. Gas Sci. Eng.* **2020**, *79*, 103369.
(16) An, P.; Xia, W.; Peng, Y.; Xie, G. Comparative filtration and dewatering behavior of vitrinite and inertinite of bituminous coal: Experiment and simulation study. *Int. J. Min. Sci. Technol.* **2021**, *31*, 233−240.
(17) Yao, Y.; Liu, D.; Che, Y.; Tang, D.; Tang, S.; Huang, W. Petrophysical characterisation of coals by low-field nuclear magnetic resonance (NMR). *Fuel* **2010**, *89*, 1371−1380.
(18) Zou, M.; Wei, C.; Huang, Z.; Wei, S. Porosity type analysis and permeability model for micro-trans-pores, meso-macro-pores and cleats of coal samples. *J. Nat. Gas Sci. Eng.* **2015**, *27*, 776−784.
(19) Lau, H. C.; Li, H.; Huang, S. Challenges and opportunities of Coalbed methane development in China. *Energy Fuels* **2017**, *31*, 4588−4602.
(20) Li, J.; Wang, S.; Lu, S.; Zhang, P.; Cai, J.; Zhao, J.; Li, W. Microdistribution and mobility of water in gas shale: A theoretical and experimental study. *Mar. Pet. Geol* **2019**, *102*, 496−507.
(21) Yu, S.; Bo, J.; Pei, S.; Jiahao, W. Matrix compression and multifractal characterization for tectonically deformed coals by Hg porosimetry. *Fuel* **2018**, *211*, 661−675.
(22) Zheng, S.; Yao, Y.; Liu, D.; Cai, Y.; Liu, Y.; Li, X. Nuclear magnetic resonance T2 cutoffs of coals: A novel method by multifractal analysis theory. *Fuel* **2019**, *241*, 715−724.
(23) Li, C.; Liu, G.; Cao, Z.; Yuan, W.; Wang, P.; You, Y. Analysis of petrophysical characteristics and water movability of tight sandstone using low-field Nuclear Magnetic Resonance. *Nat. Resour. Res.* **2019**, *29*, 2547−2573.
(24) Zou, M.; Liu, Y.; Huang, Z.; Zhang, M.; Zhang, P. Geological Control of Irreducible Water Within the Coal Matrix and Its Quantified Evaluation Model. *ACS Omega* **2020**, *5*, 9540−9549.
(25) Zhang, P.; Lu, S.; Li, J.; Chang, X. 1D and 2D Nuclear magnetic resonance (NMR) relaxation behaviors of protons in clay, kerogen and oil-bearing shale rocks. *Mar. Pet. Geol* **2020**, *114*, 104210.
(26) Meridji, Y.; Hursan, G.; Eid, M.; Balliet, R. Fluid Identification in Complex Clastic Reservoirs Using 2D NMR Maps: A Case Study from Saudi Arabia. *Saudi Arabia Section Technical Symposium and Exhibition*; Society of Petroleum Engineers, 2013.
(27) Fleury, M.; Romero-Sarmiento, M. Characterization of shales using T_1−T_2 NMR maps. *J. Pet. Sci. Eng.* **2016**, *137*, 55−62.
(28) Song, Y.; Zou, Q.; Su, E.; Zhang, Y.; Sun, Y. Changes in the microstructure of low-rank coal after supercritical CO_2 and water treatment. *Fuel* **2020**, *279*, 118493.
(29) Zhang, J.; Wei, C.; Yan, G. Stress sensitivity characterization and heterogeneous variation of the pore-fracture system in middle-high rank coals reservoir based on NMR experiments. *Fuel* **2019**, *238*, 331−344.
(30) Zhang, J.; Wei, C.; Vandeginste, V.; Ju, W.; Qin, Z.; Quan, F.; Soh Tamehe, L. Experimental simulation study on water migration and methane depressurizing desorption based on Nuclear Magnetic Resonance Technology: A case study of middle-rank coals from the Panguan Syncline in the Western Guizhou Region. *Energy Fuels* **2019**, *33*, 7993−8006.
(31) Zhang, X.; Wu, C.; Wang, Z. Experimental study of the effective stress coefficient for coal permeability with different water saturations. *J. Pet. Sci. Eng.* **2019**, *182*, 106282.
(32) Chen, S.; Tang, D.; Tao, S.; Ji, X.; Xu, H. Fractal analysis of the dynamic variation in pore-fracture systems under the action of stress using a low-field NMR relaxation method: An experimental study of coals from western Guizhou in China. *J. Pet. Sci. Eng.* **2019**, *173*, 617−629.
(33) Qin, L.; Zhai, C.; Liu, S.; Xu, J.; Wu, S.; Dong, R. Fractal dimensions of low rank coal subjected to liquid nitrogen freeze-thaw based on nuclear magnetic resonance applied for coalbed methane recovery. *Powder Technol.* **2018**, *325*, 11−20.
(34) Su, E.; Liang, Y.; Zou, Q. Structures and fractal characteristics of pores in long-flame coal after cyclical supercritical CO_2 treatment. *Fuel* **2021**, *286*, 119305.
(35) Cheng, M.; Fu, X.; Kang, J. Compressibility of different pore and Fracture Structures and Its Relationship with Heterogeneity and Minerals in Low-Rank Coal Reservoirs: An Experimental Study Based on Nuclear Magnetic Resonance and Micro-CT. *Energy Fuels* **2020**, *34*, 10894−10903.

https://doi.org/10.1021/acs.energyfuels.2c00592
Energy Fuels 2022, 36, 6130−6143